

Physical analysis of an operation of GaInAs/GaAs quantum-well vertical-cavity surface-emitting diode lasers emitting in the 1.3- μm wavelength range

ROBERT P. SARZAŁA

Laboratory of Computer Physics, Institute of Physics, Technical University of Łódź,
ul. Wólczańska 219, 93-005 Łódź, Poland; e-mail: rpsarzal@p.lodz.pl

Comprehensive three-dimensional self-consistent optical-electrical-thermal-gain physical modelling is used to simulate room-temperature continuous-wave performance characteristics of GaInAs/GaAs lasers emitting in the 1.3- μm wavelength range. The simulation takes into consideration all physical phenomena crucial for a laser operation including all important interactions between them. A real possibility to design high-performance 1.26- μm GaInAs/GaAs quantum-well vertical-cavity surface-emitting diode lasers (VCSELs) with the aid of a currently available technology is shown. Their outputs are much higher than in the case of their quantum-dot version. Methods to shift the emitting wavelength range of 1.3 μm are discussed and anticipated performance characteristics of such a 1.3- μm VCSELs are determined.

Keywords: semiconductor laser, VCSEL, GaInAs/GaAs QW.

1. Introduction

Telecommunication systems at the optical fiber window of 1.3 μm exhibit many advantages over their earlier 0.85 μm counterparts [1]. In the modern short- and medium-distance optical fibre links (< 50 km), the cost of transmitter devices represents quite a significant fraction of the total system cost. Vertical-cavity surface-emitting laser (VCSEL) structure is believed to be the most suited laser configuration for optical transmitters. It follows from its inherently single-longitudinal-mode operation, easy fibre coupling, facility in modulation and straightforward fabrication of two-dimensional arrays. Currently commercially available long-wavelength 1.3- μm diode lasers are based on (InGa)(AsP)/InP structures, often with GaAs/AlAs distributed Bragg reflector (DBR) mirrors. This solution requires a complicated growth and processing procedure which is probably too expensive for mass-produced commercial devices. Besides, since the above lasers exhibit poor temperature characteristics mainly due to insufficient electron confinement, thermoelectric coolers are required in their practical

use. Therefore, taking additionally into consideration the well established arsenide technology (GaAs/(AlGa)As/AlAs structures with GaAs/AlAs DBRs and oxidized AlAs layers), currently the most promising solution to this problem seems to be arsenide structures with such active-gain materials which are lattice matched to GaAs and emit in the 1.3 μm range. Then the whole structure could be grown in one epitaxial process which considerably reduces its costs and enables the mass manufacturing.

One of possible and, at the same time, natural ways to solve the above problem is to modify the GaAs/(AlGa)As/AlAs devices by adding the GaInAs/GaAs structures. Traditionally this system was used to manufacture devices emitting radiation of wavelengths up to 1 μm [2], recently, however, development of MBE and MOCVD technologies has enabled manufacturing devices which emit radiation of longer wavelengths. Currently GaInAs/GaAs quantum-well (QW) structures [3, 4] and based on them edge-emitting diode lasers [5, 6] emitting radiation of wavelengths even exceeding 1.2 μm are produced. To achieve such long wavelengths, InAs mole fraction should be increased to at least 40%. It is followed by a large lattice misfit reaching even +2.9% leading to considerable stresses. Efficient photoluminescence is in such structures rather difficult to achieve and needs improving the technology.

The above structures were also used to design vertical-cavity surface-emitting diode lasers (VCSELs) emitting radiation of wavelengths exceeding 1.26 μm [7, 8]. It requires waveguides of detuned spectral characteristics towards higher wavelengths with respect to the maximal-gain wavelength. It is expected that such VCSELs will be manufactured, emitting radiation of over 1 mW power and with still relatively low threshold current of the order of some milliamperes. Such lasing devices may be used as sources of a carrier wave in 10 Gbps single-mode Ethernet [9] or SONET OC-192 [10] networks.

2. Structure

The device under consideration (Fig. 1) is a typical double-intracavity-contact VCSEL structure. It consists of two 8-nm GaInAs/GaAs QWs (double QW (DQW) structure), each containing about 40% indium, separated by the 25-nm GaAs barrier, both intentionally undoped (residual 10^{16} cm^{-3} doping is assumed). The above QW structures, especially their compositions and layer thickness, are probably limiting the possible achievements of current manufacturing technologies. The active region is sandwiched by the *p*-type and the *n*-type GaAs spacers. The upper part (over the oxide aperture) of the *p*-type spacer is doped to $2 \times 10^{18} \text{ cm}^{-3}$, whereas the lower one (between the oxide and the active region) is doped only to 10^{17} cm^{-3} . Analogously, the upper part (between the active region and the base of the mesa structure) of the *n*-type spacer is doped to only 10^{16} cm^{-3} , whereas the bottom one – to 10^{18} cm^{-3} . Relatively high doping of the upper part of the *p*-type spacer and the bottom part of the *n*-type one is applied to reduce their electrical resistivities because they are also working as radial-current-spreading layers for a current flow from annular contacts towards the central active region. 28 periods of quarter-wave GaAs/Al_{0.8}Ga_{0.2}As layers (of total

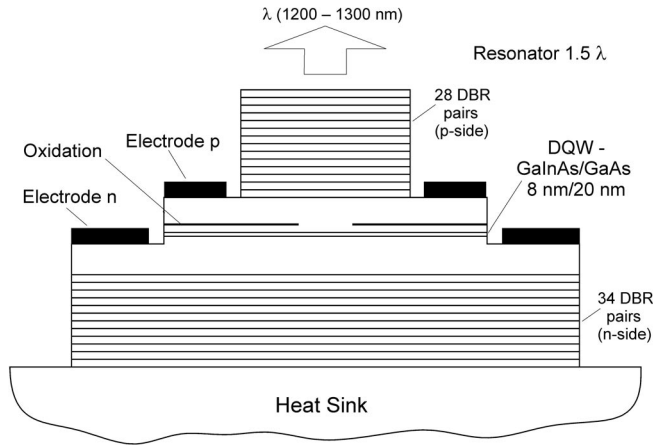


Fig. 1. Typical structure of the 1.3- μm GaAs-based oxide-confined (OC) GaInAs/GaAs double quantum-well (DQW) vertical-cavity surface-emitting laser (VCSEL).

reflectivity of 99.9350%) and analogous 34 periods of GaAs/AlAs layers (99.9943%) are assumed as upper and bottom, respectively, DBR resonator mirrors. Their diameters are equal to 50 and 100 μm , respectively. Two (*n*- and *p*-side) annular contacts are deposited on both GaAs spacer layers (see Fig. 1). Internal contact diameters are postulated to be equal to 54 μm (*p*-side) and 74 μm (*n*-side), respectively, whereas external ones – to 70 and 100 μm . Typical values of their contact resistances are equal to $10^{-5} \Omega\text{cm}^2$ (*n*-side) and $10^{-4} \Omega\text{cm}^2$ (*p*-side) (reported values, see, *e.g.*, [11, 12], are even much lower).

A radial selective oxidation (transforming AlAs into Al_xO_y native oxides) is proposed to create within the *p*-type GaAs spacer the oxide aperture working as both

T a b l e 1. Compositions and thicknesses (in nm) of structure layers of the $3\lambda/2$ -cavity VCSEL. Some values of model parameters are also given.

Layer	Wavelength	1200 nm	1250 nm	1300 nm
	Upper DBR	GaAs	87.4	91.3
$\text{Al}_{0.8}\text{Ga}_{0.2}\text{As}$		98.7	103.0	107.3
<i>p</i> -GaAs		168.2	176.2	184.1
<i>p</i> - $\text{Al}_{0.98}\text{Ga}_{0.02}\text{As}/\text{Al}_x\text{O}_y$		15	15	15
GaAs		149.6	157.6	165.4
Active region	QW-GaInAs	8	8	8
	B-GaAs	20	20	20
	QW-GaInAs	8	8	8
GaAs		76.1	84.0	91.9
<i>n</i> -GaAs		80	80	80
Bottom DBR	AlAs	102.2	106.7	111.1
	GaAs	87.4	91.3	95.3

the electrical (to funnel current spreading from annular contact towards the central active region) and the optical (to confine an optical field in a radial direction) apertures of an assumed diameter of $\phi = 2r_A$. A nominal thickness of oxide apertures is assumed to be equal to 15 nm. For all the designs, an optimal value $\phi = 4 \mu\text{m}$ was assumed.

In order to reduce the threshold current, which has happened to be very important for designing 1.3- μm GaInAs/GaAs VCSELs, a short resonator, namely the 1.5λ cavity is considered. Both the active region and the oxide aperture are assumed to be located exactly in the anti-node positions of the optical standing wave.

Compositions and thicknesses of structure layers are listed in Tab. 1 for three resonator configurations tuned, respectively, to emission of 1200, 1250 and 1300-nm radiation. For all three cases, the active region remains the same. Expected wavelengths of radiation were compelled by a suitable cavity and DBR configurations assuming high enough optical gain from tail parts of material gain spectra.

3. Model

The model is composed of five interrelated parts. In successive subsections, the band structure of the GaInAs/GaAs quantum well as well as electrical, optical, thermal and gain processes crucial for the laser operation are described, followed by an explanation of all essential interactions between various physical phenomena. General rules of the advanced modeling of a VCSEL operation are formulated by OSIŃSKI and NAKWASKI [13].

3.1. GaInAs/GaAs quantum well

Determination of a quantum-well band structure and its energy levels needs knowledge of values of the band-gaps, the effective masses and the band offset. The room-temperature (RT) value of the band-gap of the $\text{Ga}_{1-x}\text{In}_x\text{As}$ material is taken from [14] in the following form:

$$E_{\text{GaInAs}}(x, 0\text{K}) = 1.512 - 1.337x + 0.27x^2 \text{ [eV]}. \quad (1)$$

The band-gap for GaAs at 0K is found from [15]: $E_{\text{GaAs}}(0\text{K}) = 1.519 \text{ eV}$. For other temperatures, the band-gaps are determined from the Varshni relation:

$$E(T) = E(0\text{K}) - \frac{\alpha_E T^2}{\beta_E + T} \quad (2)$$

where values of α_E and β_E parameters are listed in Tab. 2.

On the basis of data reported in [16], the band offset ratio is assumed for the GaInAs/GaAs material to be equal to 0.70/0.20. The matrix element is found theoretically from Eq. (2). The electron effective mass $m_e^* = [0.026 + 0.041(1-x)]m_0$

T a b l e 2. The α_E and β_E parameters used in Eq. (2).

Material	α_E [10^{-4} eV/K]	β_E [K]
GaAs [30]	5.405	204
GaInAs [14]	5.408	204

is taken from [17], and those for the heavy hole $m_{hh}^* = (0.445 - 0.035x)m_0$ and the light hole $m_{lh}^* = 0.156m_0$ – from [18] and [19], respectively.

3.2. Electrical model

Current spreading in a laser volume is determined from three-dimensional potential distributions $V(r, z, \varphi)$ found by solving, with the aid of the finite-element (FE) method, the Laplace equation

$$\operatorname{div}\left[\sigma(r, z, \varphi)\operatorname{grad}\left(V(r, z, \varphi)\right)\right] = 0 \quad (3)$$

where σ stands for the 3D profile of electrical conductivity and r, z and φ compose the cylindrical co-ordinate system with $0z$ axis directed along the device axis. For all layers of the laser structure (with the exception of the active region), the above conductivity σ depends on material composition and its doping, as well as on a local temperature and a local carrier concentration [20]. Generation and recombination phenomena within the active region are usually a source of the non-zero right-hand side of Eq. (3) (known as the Poisson equation in this case). Their relative influence is difficult to analyze theoretically, therefore they have been taken symbolically into account in the model with the aid of the effective conductivity σ_{pn} of the active-region material. Its value is found using the differential Ohm's law and the classical diode equation:

$$\sigma_{pn}(r) = \frac{\beta_{pn}j_{pn}(r)d_{A,E}}{\ln\left[\frac{j_{pn}(r)}{j_s} + 1\right]} \quad (4)$$

where j_{pn} is the p - n junction current density and $d_{A,E} = 25 \text{ nm (GaAs)} + 2 \times 8 \text{ nm (GaInAs)} = 41 \text{ nm}$ (see Tab. 1) stands for the cumulative active-region thickness including not only QW layers but also barrier layers between them; $\beta_{pn} = 19 \text{ V}^{-1}$ is the diode parameter and $j_s = 1.1 \text{ A/m}^2$ stands for the saturation current density.

To obtain 3D potential profile for the whole laser structure, it should be matched (using the self-consistent approach) with the aid of boundary conditions at all

boundaries between the layers. Then the 3D current density distribution $j(r, z, \varphi)$ may be found within the whole device volume from the differential Ohm law:

$$j(r, z, \varphi) = -\sigma(r, z, \varphi) \text{grad}[V(r, z, \varphi)]. \quad (5)$$

Afterwards, carrier density profile $n_A(r)$ within the active layer may be determined from the below-threshold diffusion equation:

$$D_A \left[\frac{\partial^2 n_A(r)}{\partial r^2} + \frac{1}{r} \frac{\partial n_A(r)}{\partial r} \right] - An_A(r) - Bn_A^2(r) - Cn_A^3(r) + \frac{j_{pn}(r)}{ed_A} = 0 \quad (6)$$

where $D_A = 10 \text{ cm}^2/\text{s}$ is the ambipolar diffusion coefficient [21] and the recombination coefficients for temperatures within the range are extracted from the data reported in [22] in the following forms:

$$A = (138.06 - 0.109T) 10^7 \quad [\text{s}^{-1}], \quad (7a)$$

$$B = (25.35 - 0.0562T) 10^{-11} \quad [\text{cm}^3\text{s}^{-1}], \quad (7b)$$

$$C = (-6.22 + 0.0344T) 10^{-29} \quad [\text{cm}^6\text{s}^{-1}]. \quad (7c)$$

Values of the above recombination coefficients are taken from the GaInNAs measurements of a similar In content because analogous values for GaInAs have not been reported yet. A relatively high value of the A coefficient is in GaInNAs associated with a high density of nonradiative recombination centers. Expected high densities of analogous centers in GaInAs will be probably followed by a similar high value of its coefficient. Values of both remaining coefficients are not essentially different from their standard values reported for similar materials.

3.3. Optical model

The optical model is based on the effective frequency method (EFM) [23]. The structure eigenmode is assumed to be of the following form:

$$E(r, z, \varphi, t) = E(r, z, \varphi) \exp(i\omega t) \quad (8)$$

with a complex mode frequency

$$\omega = \omega' + i\omega'' \quad (9)$$

accounting for possible loss and gain effects within the optical cavity.

Assuming circular symmetry of a VCSEL geometry, the optical field may be separated into two approximating one-dimensional functions

$$E(r, z, \varphi) = f(r, z) \Phi_L(r) \exp(iL\varphi), \quad L = 0, 1, 2, \dots \quad (10)$$

where L is the azimuthal mode number. The axial part of the solution is assumed to be normalized

$$\int_0^{L_L(r)} f^2(r, z) dz = 1 \quad (11)$$

where $L_L(r)$ corresponds to the resonator length at the radius r . Finally, complex optical fields in VCSEL resonators are simplified to be governed by two mutually interrelated nearly-one-dimensional wave equations along both axial and radial directions:

$$\left[\frac{d^2}{dz^2} + k_0^2 n_R^2(r, z) \right] f(r, z) = v_{\text{eff}}(r) k_0^2 n_R(r, z) n_g(r, z) f(r, z), \quad (12)$$

$$\left[\frac{d^2}{dr^2} + \frac{1}{r} \frac{d}{dr} - \frac{L^2}{r^2} + v_{\text{eff}}(r) k_0^2 \langle n_R n_g \rangle_r \right] \Phi_L(r) = \nu k_0^2 \langle n_R n_g \rangle_r \Phi_L(r) \quad (13)$$

where v_{eff} is the effective frequency, $k_0 = \omega_0/c$ is the vacuum wave number, and ω_0 is the real-valued nominal angular frequency corresponding to the designed periodicity of DBR mirrors; $n_R(r, z, \varphi, \omega_0)$ and $n_g(r, z, \varphi, \omega_0)$ are the complex refractive phase and group indices, respectively, evaluated at the nominal angular frequency ω_0 . The dimensionless complex parameter ν plays a role of an eigenvalue and is defined as

$$\nu \equiv 2 \frac{\omega_0 - \omega}{\omega_0} = 2 \frac{\lambda - \lambda_0}{\lambda} - i \frac{2\omega''}{\omega_0}. \quad (14)$$

Its real part describes the relative wavelength shift from the nominal wavelength λ_0 , whereas its imaginary part is the relative decay constant of the corresponding mode. $\langle n_R n_g \rangle_r$ may be written in the following form:

$$\langle n_R n_g \rangle_r = \int_0^{L_L(r)} n_R(r, z) n_g(r, z) f^2(r, z) dz. \quad (15)$$

Assuming the outgoing plane waves at the bottom ($z = 0$) and the top ($z = L_L$) surfaces of the laser cavity, the following axial boundary conditions may be formulated

$$\frac{df}{dz} \pm ik_z f = 0, \quad z = \begin{cases} L_L(r) + \varepsilon \\ 0 - \varepsilon \end{cases} \quad (16)$$

where ε is a small positive number and $k_z = k_0(n_R^2 - v_{\text{eff}} n_R n_g)$. So, the structure is divided into a number of cylindrically symmetric ring sectors. Constant and uniform distributions of refractive indices and of loss and gain coefficients within every

individual layer and every individual sector are assumed – but they may be different in different layers and in different sectors.

Analogously, $\Phi_L(r)$ ($L = 0, 1, 2, \dots$) are assumed to satisfy the following boundary conditions, ensuring a cylindrical outgoing wave at sufficiently large radial distance r_∞

$$\frac{d\Phi_L(r)}{dr} + \frac{\Phi_L(r)}{2r} + ik_r\Phi_L(r) = 0 \quad (r = r_\infty) \quad (17)$$

where $k_r = k_0 \left[(v_{\text{eff}} - v) \langle n_R n_g \rangle_r \right]^{1/2}$. The radial field is determined for a structure averaged in the z -direction, as if the waveguide were uniform, although slow radial changes of losses (or gains) and refractive indices are also included.

The algorithm needs self-consistent procedure because the effective frequency v_{eff} is present in both nearly one-dimensional wave Eqs. (12) and (13).

3.4. Thermal model

The FE thermal model of the laser solves the heat-conduction equation for the whole structure using the same mesh generated for the FE electrical calculations

$$\text{div} \left[\lambda_T(r, z, \varphi) \text{grad} \left(T(r, z, \varphi) \right) \right] = -g_T(r, z, \varphi). \quad (18)$$

In the above equation, λ_T stands for the thermal conductivity coefficient ($\text{Wm}^{-1}\text{K}^{-1}$) and g_T is the volume density of heat sources (Wm^{-3}). Thermal conductivity of the oxidized Al_xO_y layer is assumed equal to that of the sapphire (Al_2O_3) – 19.65 W/mK [24] and that of semiconductor layers are taken from [25]. Nonradiative recombination and reabsorption of spontaneous radiation are found to be main heat sources located within the active region of the laser. Additionally, the volume Joule heating in all structure layers and the barrier Joule heating in the contacts are taken into account. 3D heat-flux spreading in a copper heat sink is determined assuming its external walls to be kept at the RT of the ambient. Side and top laser-crystal walls are assumed to be thermally isolated because an influence of both thermal radiation and thermal convection of air particles is negligible as compared with intense heat-flux conduction through the bottom device base into its heat sink.

3.5. Gain model

In the calculation of the optical gain, the classical Fermi's Golden Rule and the parabolic band-gap approximation are assumed [26]. The optical gain spectra g may be then determined from the following relation:

$$g(\hbar\omega) = \sum_m \int_{-\infty}^{\infty} g_m(\varepsilon) A(\hbar\omega - \varepsilon) d\varepsilon \quad (19)$$

where the summation should be carried out over all available numbers m of level pairs, and

$$g_m(\hbar\omega) = \frac{e^2 \pi \hbar}{n_R c m_0^2 \varepsilon_0} \frac{|M|^2 \rho_r^{2D}(\hbar\omega)}{\hbar\omega} \left\{ f_c[E_e(m, \hbar\omega)] - f_v[E_h(m, \hbar\omega)] \right\} \quad (20)$$

where n_R stands for the index of refraction, c is the speed of light in vacuum, m_0 is the rest electron mass, ε_0 is the vacuum dielectric constant, M is the momentum matrix element, ρ_r^{2D} stands for the two-dimensional reduced density of states, f_c and f_v are the Fermi–Dirac functions determined for electrons in the conduction band and for holes in the valence band, respectively, E_e and E_h are energies of the recombining electron and hole, respectively, and A is the broadening function [27], usually of the Lorentzian type.

The momentum matrix element $|M|^2$, known from the Fermi's Golden Rule, describes the interaction between the electromagnetic wave and carriers. For the electron–heavy hole transitions and the TE polarization, the following expression resulted from the Kane model [26]:

$$|M|^2 = \frac{3}{2} \left(\frac{1}{m_o^*} - 1 \right) E_g \frac{E_g + \Delta_{SO}}{E_g + \frac{3}{2} \Delta_{SO}} \quad (21)$$

where m_o^* is the electron effective mass, E_g stands for the active-region energy gap and Δ_{SO} is the spin-orbit splitting. However, experimentally determined $|M|^2$ values may be essentially different from those calculated using Eq. (21) because of some simplifications of the Kane model.

3.6. Interactions between individual physical phenomena

Our model considers all important interactions between individual physical phenomena, including:

- thermal focusing, *i.e.*, the temperature dependence of refractive indices;
- temperature dependence of thermal conductivities;
- temperature, dopant and carrier-concentration dependences of electrical conductivities;
- temperature and carrier-concentration dependences of the active-region energy gap.

Accordingly, 3D profiles of all model parameters are determined not only on a basis of various chemical compositions of structure layers but also taking into account 3D profiles of temperature, current density, radiation intensity, and carrier concentration within a whole device volume, all of them with the aid of a self-consistent calculation algorithm shown in Fig. 2.

4. Results

Traditional 980-nm GaAs-based diode lasers with GaInAs/GaAs QWs exhibit a very good thermal behaviour which follows from high values of their T_o parameter

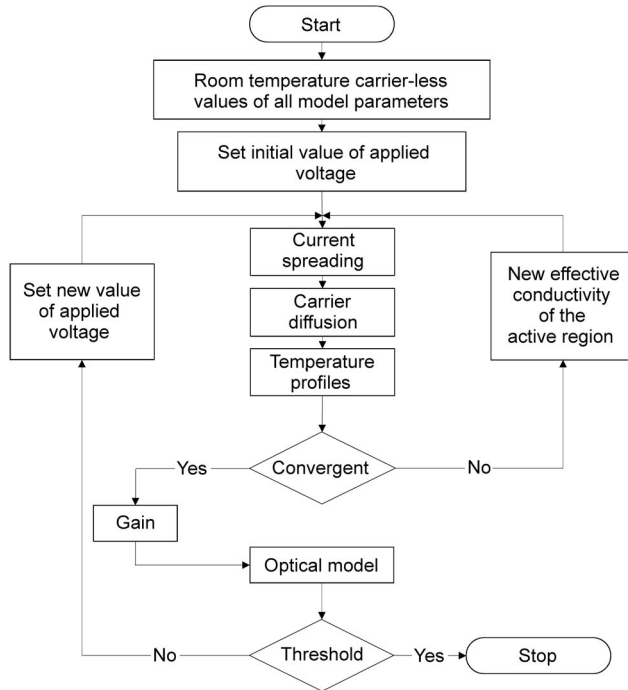


Fig. 2. Flow chart of the numerical calculation.

describing temperature dependence of a threshold current. Analogous properties should be also expected for considered new configurations of these devices, especially for their resonators tuned to the maximal active-region optical gain. Such a behaviour is confirmed by Fig. 3a presenting nearly insignificant temperature-induced threshold-current increases. For the cavity tuned to the 1200-nm wave, the characteristic T_o parameter is as high as 191 K for the (300 K, 350 K) temperature range and still high 133 K for (350 K, 390 K) one. Such a good thermal stabilisation of a threshold current follows from a high optical gain tuned to the cavity. Its value remains below 0.5 mA up to the active-region temperature of 360 K.

Detuning of the resonator from the maximal active-region gain value is followed by a considerable RT threshold current increase: to 0.67 mA for the cavity tuned to 1250 nm (Fig. 3b) and to a much higher value for the 1300-nm cavity (Fig. 3c). As expected, this current rapidly decreases with an increase in temperature, reaching for the 1250-nm cavity values below 0.35 mA for $T = (325 \text{ K}, 355 \text{ K})$ and below 1 mA for $T = (402 \text{ K}, 480 \text{ K})$ for the 1300-nm cavity. Its further increase is relatively slow ($T_o = 247 \text{ K}$ and 172 K , respectively, for both the above cases). This behaviour is a direct consequence of temperature-induced shifting of the active-region optical gain towards longer wavelengths, which is followed by a better tuning to laser cavities

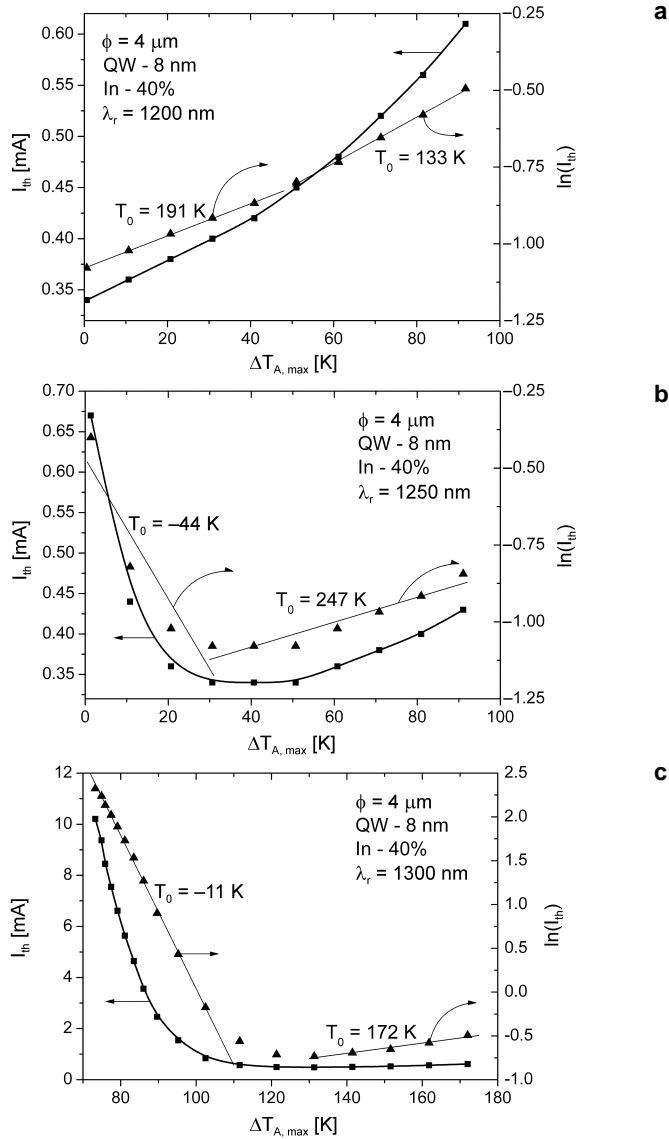


Fig. 3. Threshold current I_{th} as a function of the active-region temperature increase $\Delta T_{A, \text{max}}$ over the room temperature $\text{RT} = 300 \text{ K}$ determined for VCSEL structures designed for the lasing wavelength: 1200 nm (a), 1250 nm (b), 1300 nm (c). Values of the T_0 characteristic temperature are indicated. Active regions are the same in all VCSEL structures.

(Fig. 4). As one can see in Fig. 3b and Fig. 4a, the considered VCSEL design seems to exhibit high performance as the 1250-nm laser source for a wide temperature range.

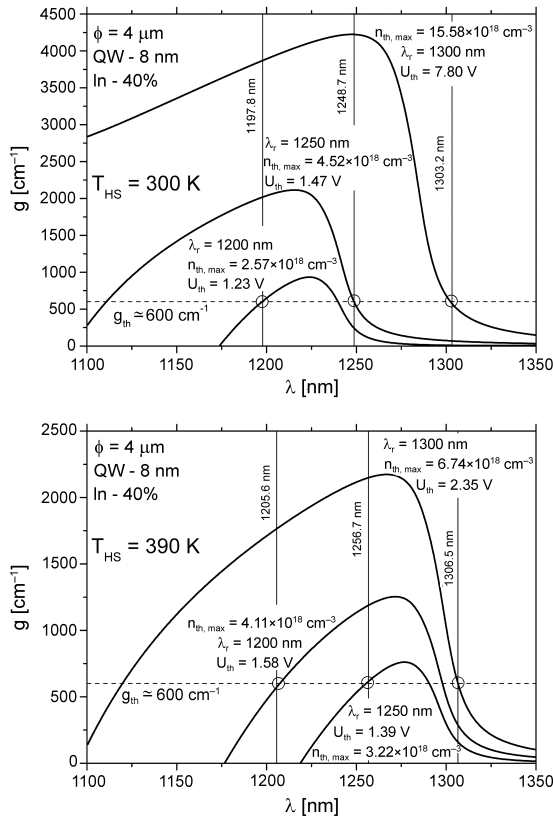


Fig. 4. Gain spectra $g(\lambda)$ of the $\text{Ga}_{0.6}\text{In}_{0.4}\text{As}/\text{GaAs}$ 8-nm quantum well determined for lasing-threshold conditions and two ambient temperatures: 300 K (a) and 390 K (b). Threshold voltage U_{th} and maximal values of threshold carrier concentration $n_{\text{th,max}}$ are indicated. Assumed threshold gain of 600 cm^{-1} is shown.

Analogous performance of the 1300-nm VCSEL does not meet our expectation. Its RT operation is possible only for very high operation currents, which excludes its practical significance.

Figure 4 presents active-region gain spectra for selected operation conditions. Perpendicular lines correspond to resonator wavelengths. Their intersections (identified by small circles) indicate values of an optical gain available for considered designs and temperatures. Both the gain spectrum and the cavity characteristic are shifted with an increase in temperature towards longer wavelengths. But the gain spectrum (dependent on the energy gap) is shifted much more rapidly than the cavity wavelength (dependent on refractive indices and thermal expansion). For the 1200-nm cavity, the former peak is shifted at the rate of 0.52 nm/K , whereas the latter one – 0.085 nm/K , which is seen comparing Fig. 4a and 4b.

At 300 K (Fig. 4a), the gain spectrum of the 1200-nm laser is quite well tuned to the laser cavity which is followed by its very low lasing threshold. Besides, an increase in the active-region temperature causes a move of the working point along the gentle-slope side of the gain spectrum. Therefore, an increase in the ambient temperature causes a relatively slow threshold-current increase, which is a reason of a very high T_o value of the 1200-nm laser just over RT (Fig. 3a).

Gain spectrum of the 1250-nm laser is at RT (Fig. 4a) much more detuned from its cavity wavelength which is followed by a much higher lasing threshold to raise the whole gain spectrum. But fortunately with an increase in temperature the gain spectrum is becoming closer and closer to the cavity wavelength, so the detuning is steadily reduced. It is followed by a rapid decrease in the lasing threshold (Fig. 3b): the best tuning is achieved between 330 K and 350 K, after which a relatively slow threshold increase is observed ($T_o = 247$ K).

Initial detuning at RT of the 1300-nm laser is very large (Fig. 4a). Its working point is situated far from the gain maximum. In this case an increase in the whole gain spectrum to reach the lasing threshold would need the extremely high threshold carrier concentration. Fortunately, an increase in the active-region temperature, being a result of high operation currents, causes an additional shift of the gain spectrum towards longer wavelengths. Nevertheless RT lasing threshold determined for this structure (Fig. 4a) is very high: RT threshold voltage is very low for the 1200-nm laser – 1.23 V, remains still quite low for the 1250-nm laser – 1.47 V, but is surprisingly high for the 1300-nm laser – 7.80 V.

Radial profiles of the threshold carrier concentration j_{th} and the active-region temperature increase $T_A - T_{HS}$ are plotted in Fig. 5 for the 1300-nm laser. As one can see, temperature profiles remain within the active-region $r < 2 \mu\text{m}$ area relatively uniform for all considered ambient temperatures T_{HS} . Current density, on the other

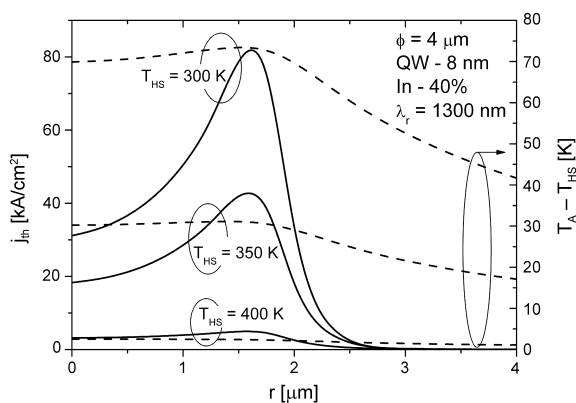


Fig. 5. Radial profiles of the p - n junction current density j_{th} and the active-region temperature increase $T_A - T_{HS}$ determined for various ambient temperature T_{HS} .

hand, becomes more and more nonuniform with an increase in T_{HS} . Lower threshold current densities are shown at higher temperatures because an increase in temperature is followed by better matching of the cavity wavelengths and the active-region gain spectrum (*c.f.* Figs. 4a and 4b), therefore the threshold current is reduced (Fig. 3c). As expected, a distinct current-crowding effect is seen close to the active-region edge, especially at RT. This effect would be much more pronounced in VCSELs with larger active regions, which was analysed in earlier author's papers [28, 29]. Therefore, to optimise this structure for a possible 1300-nm emission, relatively small active region has been chosen.

5. Conclusions

Physical aspects of an operation of GaAs-based GaInAs/GaAs QW VCSELs have been considered in the present paper using the comprehensive three-dimensional self-consistent optical-electrical-thermal-gain simulation. A possibility of designing 1.3- μm devices has been analysed. Currently available technology has been confirmed to enable manufacturing the above devices emitting radiation of wavelengths over 1.2 μm . In GaAs-based structures, very good DBR resonator mirrors and very efficient methods to confine radially both the current spreading and the electromagnetic field with the aid of oxide apertures may be applied.

While high-performance 1.26- μm QW GaInAs/GaAs VCSELs may be produced using even currently available and still immature technology, analogous 1.3- μm devices seem to be still beyond its capability. Nevertheless the former devices of much higher output than their quantum-dot versions may be already used in 10 Gbps single-mode Ethernet [9] or SONET OC-192 [10] networks. It may be also expected that improved technology in future may enable also manufacturing 1.3- μm VCSELs.

Acknowledgements – This work has been supported by the Polish State Committee for Scientific Research (KBN), grants No. 7-T11B-073-21 and No. 4-T11B-014-25.

References

- [1] SARZALA R.P., *Computer simulation of performance characteristics of (GaIn)(NAs) diode lasers*, *Optica Applicata* **32**(3), 2002, pp. 449–60.
- [2] KOYAMA F., SCHLENKER D., MIYAMOTO T., CHEN Z., MATSUTANI A., SAKAGUCHI T., IGA K., *Data transmission over single-mode fiber by using 1.2- μm uncooled GaInAs-GaAs laser for Gb/s local area network*, *IEEE Photonics Technology Letters* **12**(2), 2000, pp. 125–7.
- [3] HARMAND J.C., LI L.H., PATRIARCHE G., TRAVERS L., *GaInAs/GaAs quantum-well growth assisted by Sb surfactant: Toward 1.3 μm emission*, *Applied Physics Letters* **84**(20), 2004, pp. 3981–3.
- [4] NI H.Q., NIU Z.C., XU X.H., XU Y.Q., ZANG W., WEI X., BIAN L.F., HE Z.H., HAN Q., WU R.H., *High-indium-content $\text{In}_x\text{Ga}_{1-x}\text{As}/\text{GaAs}$ quantum wells with emission wavelengths above 1.25 μm at room temperature*, *Applied Physics Letters* **84**(25), 2004, pp. 5100–2.

- [5] MOGG S., PLAINE G., ASPLUND C., SUNDGREN P., BASKAR K., MULOT M., SHATZ R., HAMMAR M., *High-performance 1.2- μm Highly strained InGaAs/GaAs quantum well lasers*, Conference Proceedings – International Conference on Indium Phosphide and Related Materials, 2002, pp. 107–10.
- [6] SUNG L.W., LIN H.H., *Highly strained 1.24- μm InGaAs/GaAs quantum-well lasers*, Applied Physics Letters **83**(6), 2003, pp. 1107–9.
- [7] ASPLUND C., SUNDGREN P., MOGG S., HAMMAR M., CHRISTIANSSON U., OSCARSSON V., RUNNSTRÖM C., ODLING E., MALMQUIST J., *1260 nm InGaAs vertical-cavity lasers*, Electronics Letters **38**(13), 2002, pp. 635–6.
- [8] SCHLENKER D., MIYAMOTO T., CHEN Z.B., KAWAGUCHI M., KONDO T., GOUARDES E., KOYAMA F., IGA K., *Critical layer thickness of 1.2- μm highly strained GaInAs/GaAs quantum wells*, Journal of Crystal Growth **221**, 2000, pp. 503–8.
- [9] KUDO M., MISHIMA T., *Improved photoluminescence properties of highly strained InGaAs/GaAs quantum wells grown by molecular-beam epitaxy*, Journal of Applied Physics **78**(3), 1995, pp. 1685–8.
- [10] ROAN E.J., CHENG K.Y., *Long-wavelength (1.3 μm) luminescence in InGaAs strained quantum-well structures grown on GaAs*, Applied Physics Letters **59**(21), 1991, pp. 2688–90.
- [11] ABOELFOTOH M.O., BORAK M.A., NARAYAN J., *Ohmic contact to p-type GaAs using Cu_3Ge* , Applied Physics Letters **75**(25), 1999, pp. 3953–5.
- [12] UENG U.J., CHEN N.-P., JANES D.B., WEBB K.J., MCINTURFF D.T., MELLOCH M.R., *Temperature-dependent behavior of low-temperature-grown GaAs nonalloyed ohmic contacts*, Journal of Applied Physics **90**(11), 2001, pp. 5637–41.
- [13] OSIŃSKI M., NAKWASKI W., [In] *Vertical-Cavity Surface-Emitting Laser Devices*, [Eds.] E.H. Li, K. Iga, Series on Photonics, Vol. 6, Springer, Berlin, Heidelberg 2003, p. 135.
- [14] SKIERBISZEWSKI C., *Experimental studies of the conduction-band structure of GaInNAs alloys*, Semiconductor Science and Technology **17**(8), 2002, pp. 803–14.
- [15] BLAKEMORE J.S., *Semiconducting and other major properties of gallium arsenide*, Journal of Applied Physics **53**(10), 1982, pp. R123–81.
- [16] CHOW W.W., JONES E.D., MODINE N.A., ALLERMAN A.A., KURTZ S.R., *Laser gain and threshold properties in compressive-strained and lattice-matched GaInNAs/GaAs quantum wells*, Applied Physics Letters **75**(19), 1999, pp. 2891–3.
- [17] VURGAFTMAN I., MEYER J.R., RAM-MOHAN L.R., *Band parameters for III–V compound semiconductors and their alloys*, Journal of Applied Physics **89**(11), 2001, pp. 5815–75.
- [18] MOUMANIS K., SEISYAN R.P., KOKHANOVSKII S.I., SASIN M.E., *Light and heavy hole excitons in absorption and magnetoabsorption spectra of InGaAs/GaAs MQWs*, Thin Solids Films **364**(1-2), 2000, pp. 249–53.
- [19] LANCEFIELD D., ADAMS A.R., MENY A.T., KNAP W., LITWIN-STASZEWSKA E., SKIERBISZEWSKI C., ROBERT J.L., *Light-hole mass in a strained InGaAs/GaAs single quantum well and its pressure dependence*, Journal of Physics and Chemistry of Solids **56**(3-4), 1995, pp. 469–73.
- [20] NAKWASKI W., OSIŃSKI M., *Thermal analysis of GaAs-AlGaAs etched well surface-emitting double-heterostructures lasers with dielectric mirrors*, IEEE Journal of Quantum Electronics **29**(6), 1993, pp. 1981–95.
- [21] SARZAŁA R.P., NAKWASKI W., *Carrier diffusion inside active regions of gain-guided vertical-cavity surface-emitting lasers*, IEE Proceedings: Optoelectronics **144**(6), 1997, pp. 421–5.
- [22] FEHSE R., TOMIĆ S., ADAMS A.R., SWEENEY S.J., O'REILLY E.P., ANDREEV A., RIECHERT H., *A quantitative study of radiative, auger, and defect related recombination processes in 1.3- μm GaInNAs-based quantum-well lasers*, IEEE Journal of Selected Topics in Quantum Electronics **8**(4), 2002, pp. 801–10.

- [23] WENZEL H., WÜNSCHE H.-J., *The effective frequency method in the analysis of vertical-cavity surface-emitting lasers*, IEEE Journal of Quantum Electronics **33**(7), 1997, pp. 1156–62.
- [24] ALEXANDER W., SHACKELFORD J., *Materials Science and Engineering Handbook*, CRC Press 2000.
- [25] NAKWASKI W., *Thermal conductivity of binary, ternary, and quaternary III-V compounds*, Journal of Applied Physics **64**(1), 1988, pp. 159–66.
- [26] CHUANG S.L., *Physics of Optoelectronics Devices*, Wiley, New York 1995.
- [27] ELISEEV P.G., *Line shape function for semiconductor laser modelling*, Electronics Letters **33**(24), 1997, pp. 2046–8.
- [28] SARZAŁA R.P., *Modeling of the threshold operation of 1.3- μm GaAs-based oxide-confined (InGa)As-GaAs quantum-dot vertical-cavity surface-emitting lasers*, IEEE Journal of Quantum Electronics **40**(6), 2004, pp. 629–34.
- [29] SARZAŁA R.P., NAKWASKI W., *Optimization of 1.3 μm GaAs-based oxide-confined (GaIn)(NAs) vertical-cavity surface-emitting lasers for low-threshold room-temperature operation*, Journal of Physics: Condensed Matter **16**(31), 2004, S3121–40.
- [30] THURMOND C.D., *Standard thermodynamic functions for the formation of electrons and holes in Ge, Si, GaAs, and GaP*, Journal of the Electrochemical Society **122**(8), 1975, pp. 1133–41.

Received December 9, 2004